中国激光

平顶飞秒激光开槽硅晶圆工艺仿真与实验研究

张喆[1,2]，宋琦[1,3]，张昆鹏[1]，薛美[1]，侯煜[1**]，张紫辰[1*]

[1]中国科学院微电子研究所微电子仪器设备研发中心，北京 100029；

[2]中国科学院大学微电子学院，北京 100049；

[3]长春理工大学国家纳米测量与制造技术中心，吉林 长春 130022

摘要 硅是半导体领域使用最广泛的材料，近几年随着制程工艺的发展，传统的机械划片方法已经无法满足更高的加工质量要求。现有激光开槽与金刚石刀结合的划片工艺，多采用纳秒多光束的激光加工方式。介绍了能量呈平顶分布的飞秒激光开槽硅晶圆技术的双温数值仿真模型与实验，使用波长为 517 nm 的飞秒激光，基于有限元模型分析了飞秒脉冲加热硅表面的能量沉积过程和热场的演化过程，研究了激光功率、光斑间隔和能量分布等激光加工参数对工艺效果的影响。最后通过实验，实现了硅晶圆表面槽宽可控、槽底均匀、槽侧壁陡直的开槽工艺。实验结果表明，平顶飞秒激光划槽工艺在未来硅晶圆划片及微结构制备中具有很大的工程应用潜力。

关键词 激光技术；飞秒激光；双温模型；光束整形；激光烧蚀；晶圆划片

中图分类号 TN24 **文献标志码** A **DOI**：10.3788/CJL230518

1 引 言

硅在生物、能源特别是集成电路领域中发挥着重要作用[1-3]。在封装划片领域，随着半导体制造逐步向大幅面、薄衬底等方向发展，传统刀片划片造成的晶片崩边及破损对良品率的影响越来越严重[4-5]。随着激光技术的发展，业界开发了许多新的激光划片技术[6-7]，以满足高产量、高边缘质量和低成本的要求。水导激光划片技术[8]用水柱作为波导，水流既可以导光又可以冲走加工碎屑。然而，水流会严重影响光场色散情况，水流冲击也会对硬脆材料带来额外的损伤风险。隐形划片技术[9-13]是将激光入射至透明衬底的中间部分，形成改质层，通过裂片分离方式完成划片加工，整个设备不需要刀片，几乎不产生碎屑。通过多焦点激光整形等手段还可以极大地提高加工效率以及激光利用率[14]。但是，隐形划片对晶圆表面有较高的要求，晶圆衬底材料及其表面的膜层限制了激光的波长选择范围，且划片道表面如果含有金属层或钝化层也会严重影响激光的聚焦效果。

激光烧蚀划片早期主要采用大功率纳秒或连续激光在晶圆表面进行烧蚀，工艺热影响区域大，容易发生熔融物冷凝堆积[15-16]，对芯片电性能和力学强度造成不良影响。近几年随着超短脉冲激光技术的不断发展，在利用超短脉冲激光作用材料表面制备微-纳米结构的研究中，选择性材料去除一直是研究热点[17-18]。Ngoi 等[19]利用皮秒激光切割硅，与长脉冲激光相比，皮秒激光对材料的损伤较小，但仍然会产生较为明显的热效应。飞秒激光峰值功率更高，在光脉冲与物质相互作用的过程中，瞬时的高能量密度沉积将使电子的吸收和动力学特性发生改变，避免了激光线性吸收能量转移和扩散等的影响，热损伤大大降低[20-21]，是实现小型化和薄型化半导体晶圆划切的最优手段。Crawford 等[22]研究了飞秒激光偏振态对硅上刻槽形貌的影响。Domke 等[23]发现较短的激光脉冲宽度有助于获得较高的硅切割后的抗弯强度。Amer 等[24]发现飞秒激光加工后硅表面的非晶化程度低于长脉冲激光加工，证明了脉冲宽度较短的激光更有利于保证材料的性质。

自从集成电路技术节点进入 90 nm 以来，低介电常数材料的引入对晶圆划片和封装工艺提出了重大挑战，业界通过激光表面开槽与机械切割相结合的方式解决划片过程中低介电常数材料的分离问题，激光脉宽也从纳秒激光逐步向飞秒激光推进。然而，现有研究多集中在激光功率、频率、散焦和加工速度的优化，以及多光束激光划片光斑分布的工艺对比，理论分析尚不充分[25]。因此，本文以中心波长为 517 nm 的飞秒激光器作为光源，利用衍射光学元件将焦点光斑能量整形为平顶分布，并将其用于硅材料的表面开槽加工，从理论和实验两方面研究了激光开槽工艺的机制及槽形质量。

收稿日期：2023-02-13；**修回日期**：2023-03-19；**录用日期**：2023-04-03；**网络首发日期**：2023-04-13

基金项目：国家自然科学基金(61905273)

通信作者：*zz241@ime.ac.cn；**houyu@ime.ac.cn

2　飞秒脉冲激光与硅相互作用的数值仿真

双温模型是描述飞秒与金属材料相互作用的经典模型，飞秒辐照半导体材料时会产生强烈的非线性吸收效应，因此会引起材料表面局部电子瞬态变化。本文首先利用双温模型与过剩载流子平衡方程，建立了飞秒激光烧蚀硅材料的理论模型，模拟了平顶激光烧蚀硅材料的弹坑形貌的形成过程。最后，计算了不同光斑间隔和不同能量的多脉冲激光对开槽形貌及质量的影响。

2.1　飞秒激光烧蚀硅的理论模型

飞秒激光具有极高的峰值功率，当入射的光子能量大于禁带宽度时，单光子、双光子以及多光子吸收会同时发生，对于以硅为代表的具有间接带隙的半导体，为了满足动量守恒，需要声子辅助价带电子跃迁至导带。此外，处于导带高能带的电子通过碰撞电离，将能量传递给价带电子，进一步增加了自由载流子的浓度。在飞秒激光激发自由电子数量增加的同时，还发生辐射复合、俄歇复合、缺陷或表面复合等一系列复合，最终系统回到平衡状态。综上所述，飞秒激光与硅材料作用时载流子浓度的瞬态变化行为可以描述为

$$\frac{\partial N}{\partial t}=\frac{\alpha I}{\hbar\omega}+\frac{\beta I^2}{2\hbar\omega}+\nabla\cdot\boldsymbol{J}+\delta N-\gamma N^3, \tag{1}$$

式中：N为电子浓度；α为单光子吸收系数；β为双光子吸收系数；I为激光强度；$\hbar$为约化普朗克常量；ω为入射激光频率；$\boldsymbol{J}$为电子流密度；δ为碰撞电离系数；γ为俄歇复合系数。其中，电子流密度可以表示为

$$\boldsymbol{J}=D_0\left(\nabla N+\frac{2N}{k_{\mathrm{B}}T_{\mathrm{e}}}\nabla E_{\mathrm{g}}+\frac{N}{2T_{\mathrm{e}}}\nabla T_{\mathrm{e}}\right), \tag{2}$$

式中：D_0为双极扩散系数；k_{B}为Boltzmann常数；T_{e}为电子温度；E_{g}为禁带宽度，受到晶格温度和电子密度的影响。硅的禁带宽度一般描述为

$$E_{\mathrm{g}}(T_{\mathrm{l}})=1.16-7.02\times10^{-4}\frac{T_{\mathrm{l}}^2}{T_{\mathrm{l}}+1108}-1.5\times10^{-8}N^{\frac{1}{3}}, \tag{3}$$

式中：T_{l}为晶格温度。除禁带宽度外，碰撞电离系数$\delta=3.6\times10^{-10}\exp\left[-1.5E_{\mathrm{g}}/(k_{\mathrm{B}}T_{\mathrm{e}})\right]$，双极扩散系数$D_0=1.8\times10^{-3}\times300/T_{\mathrm{l}}$，均为温度的函数。

在自由载流子浓度升高的过程中，载流子也会通过声子的作用将能量传递给晶格，其弛豫时间为数十皮秒级别。当激光脉冲持续时间小于电子与晶格的弛豫时间时，能量会集中在电子系统中，使得电子温度和晶格温度处于非平衡状态。这一过程通常采用基于玻尔兹曼输运方程的双温模型进行描述。在双温模型中，电子和晶格被分成两个子系统。电子系统温度和晶格系统温度的瞬态演化过程分别描述为

$$\frac{\partial(NE_{\mathrm{g}}+C_{\mathrm{e}}T_{\mathrm{e}})}{\partial t}=\nabla\cdot(k_{\mathrm{e}}\nabla T_{\mathrm{e}})-\kappa(T_{\mathrm{e}}-T_{\mathrm{l}})+\alpha I+\beta I^2+N\theta I, \tag{4}$$

$$C_{\mathrm{l}}\frac{\partial(T_{\mathrm{l}})}{\partial t}=\nabla\cdot(k_{\mathrm{l}}\nabla T_{\mathrm{l}})+\kappa(T_{\mathrm{e}}-T_{\mathrm{l}}), \tag{5}$$

式中：C_{e}和C_{l}分别为电子和晶格系统的热容；k_{e}和k_{l}分别为电子和晶格系统的热导率；κ为电子-晶格热耦合系数；θ为自由电子吸收系数。其中大部分参数是随温度和载流子变化的函数：

$$C_{\mathrm{e}}=3Nk_{\mathrm{B}}+N\frac{\partial E_{\mathrm{g}}}{\partial T_{\mathrm{e}}}, \tag{6}$$

$$C_{\mathrm{l}}=1.978\times10^6+354T_{\mathrm{l}}-3.68\times10^6\frac{1}{T_{\mathrm{l}}^2}, \tag{7}$$

$$k_{\mathrm{e}}=(7.13T_{\mathrm{e}}-556)\times10^{-5}, \tag{8}$$

$$k_{\mathrm{l}}=1585T_{\mathrm{l}}^{-1.23}, \tag{9}$$

$$\kappa=\frac{3Nk_{\mathrm{B}}}{240\left[1+\left(\frac{N}{6\times10^{20}}\right)^2\right]}, \tag{10}$$

$$\theta=5\times10^{22}\frac{T_{\mathrm{l}}}{300}。 \tag{11}$$

由式(1)～(11)构建的理论模型可较为精确地描述飞秒激光烧蚀Si材料的机理，其中式(4)、(5)是核心，其他参数方程可以适当简化，或采用实验数据，在接近实际的情况下简化模型计算量。

2.2　一维单脉冲激光烧蚀的数值仿真

当激光照射材料时，价带电子通过带间跃迁吸收能量等于或高于材料的带隙能($\hbar\omega\geqslant E_{\mathrm{g}}$)的光子，同时跃迁至导带。Si材料的禁带宽度为1.12 eV，波长为517 nm的激光光子能量约为2.40 eV，单个光子可以克服Si间接带隙能量。Glezer等[26]认为，当飞秒激光能量密度大于0.05 J/cm^{2}时，半导体材料内会发生超快电子跃迁。在此过程中，大量价带电子被激发到导带，跃迁导致带隙消除，自由电子进一步吸收激光能量，半导体受辐照部分呈现类似金属的行为，单光子吸收成为主要的吸收机制[27-28]。综上所述，本实验忽略双光子吸收系数β和自由电子吸收系数θ，材料相关参数如表1所示。

表1　材料参数

Table 1　Material parameters

Parameter	Value
Absorption coefficient α /(10^6 m^{-1})	1.22
Initial electron density N_{eq} /(10^{12} cm^{-1})	1.00
Auger recombination coefficient γ /(10^{-43} m$^6\cdot$s^{-1})	3.80

本实验首先利用基于有限元方法(FEM)的数值模拟软件COMSOL Multiphysics建立一个一维模型，仿真研究飞秒激光引发Si材料表面的电子密度、电子温度和晶格温度的时域演化特性，模型长度为20 μm，

左端点边界条件设置为热绝缘，右端点边界条件为恒定激光能量，如图 1 所示。

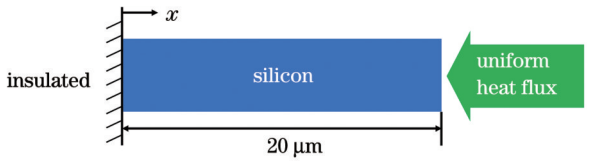

图 1　一维硅飞秒烧蚀示意图

Fig. 1　Schematic of one-dimensional silicon irradiated by femtosecond laser pulse

当激光入射材料时，激光光强的空间和时间分布可以表示为

$$I(x,y,t)=\sqrt{\frac{4\ln 2}{\pi}}\frac{(1-R)}{t_p}I_0 f_1(x,y)f_2(z)f_3(t), \tag{12}$$

式中：R 为材料表面反射率；t_p 为激光脉宽；I_0 为脉冲峰值能量密度；$f_1(x,y)$、$f_2(z)$、$f_3(t)$ 为三个指数函数，分别表示激光能量的空间分布、透射衰减以及时间分布。在一维模型中采用恒定激光能量入射，并且本实验采用的 517 nm 激光波长不会在硅材料内产生透射，即一维模型只需要考虑时间分布，模型中脉冲的时间分布呈高斯型：

$$f_3(t)=\exp\left[-4\frac{(t-t_0)^2}{t_p^2}\ln 2\right], \tag{13}$$

式中：t_0 为脉冲峰值到达时间。模型中的激光参数如表 2 所示。

表 2　激光相关参数

Table 2　Laser related parameters

Parameter	Value
Wavelength λ /nm	517
Pulse duration t_p /fs	250
Reflectivity R	0.72
Peak power density I_0 /(10^{16} W·m^{-2})	1.18

在以上参数作用下，硅材料表面的电子密度瞬态演化及电子和晶格系统的温度变化如图 2～4 所示。仿真结果显示，飞秒激光作用于 Si 表面的瞬间就激发出了大量的自由电子，电子密度在飞秒激光脉冲宽度的时间尺度内达到了最大值，之后开始缓慢下降，自由电子能在较长的时间尺度内维持较高的浓度。

由图 3 可见，Si 材料在受到飞秒激光辐照时，自由电子的温度急剧上升，在脉冲持续时间内达到最大值，最高可达到 28000 K，而此时晶格保持初始温度。随着时间的推移，电子的温度逐渐降低，晶格的温度逐渐升高。进一步分析发现，电子温度存在两个急剧升高的状态。第一个发生在脉冲前沿的 10 fs 时间尺度内，主要是材料本征载流子的自由电子吸收导致电子热导

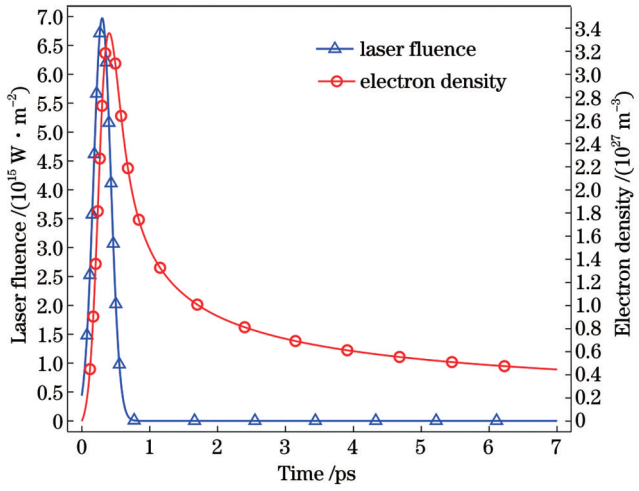

图 2　飞秒脉冲作用下硅表面电子密度的变化

Fig. 2　Variation of electron density on silicon surface under femtosecond pulse irradiation

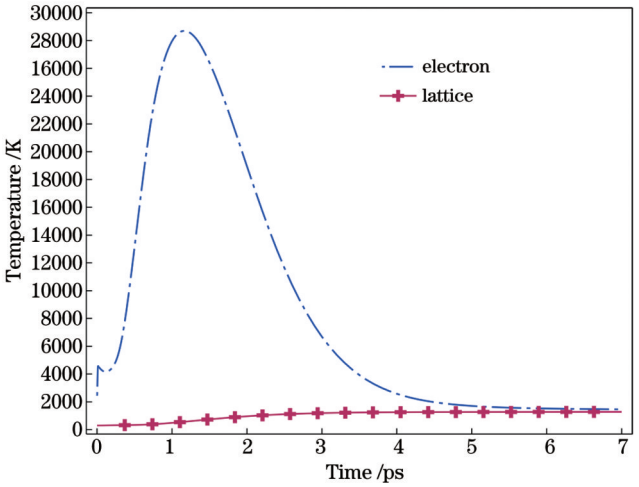

图 3　电子系统和晶格系统的温度演化

Fig. 3　Temperature evolution of electron and lattice systems

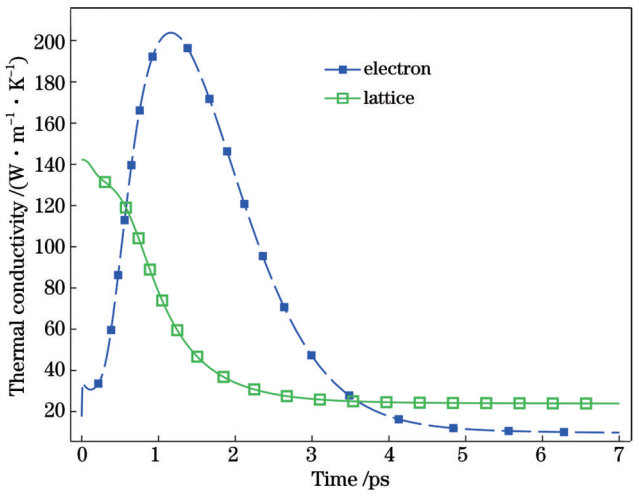

图 4　系统热导率的变化

Fig. 4　Evolution of thermal conductivity of system

率升高，如图 4 所示。第二个发生在主脉冲持续阶段，晶格耦合电子能量的速率随着自由电子密度的升高而

增大，导致电子升温的速率降低，曲线斜率趋于平缓。

通过以上仿真发现，飞秒激光照射硅材料期间晶格的温度几乎没有改变，脉冲过后电子能量缓慢向晶格系统转移。由此可以判断，517 nm 飞秒激光主要是以电子激发形式达到“冷”加工的效果，减小材料热损伤。

2.3　二维多脉冲激光烧蚀的数值仿真

将一维模型扩展为二维模型，以预测脉冲烧蚀的弹坑形貌。传统开槽工艺一般采用小能量高斯光斑进行多次加工以实现一定宽度的开槽效果，高斯小光斑开槽后槽底粗糙度一般较高，槽形较差，如图 5 所示。本文采用衍射光学元件（DOE）将激光整形为方平顶分布以用于激光开槽工艺。平顶光束加工可以解决高斯光束加工槽形差的问题，不仅可以获得一致性高的槽形，还可以减小光斑重叠率，并提高激光能量利用率和生产效率。

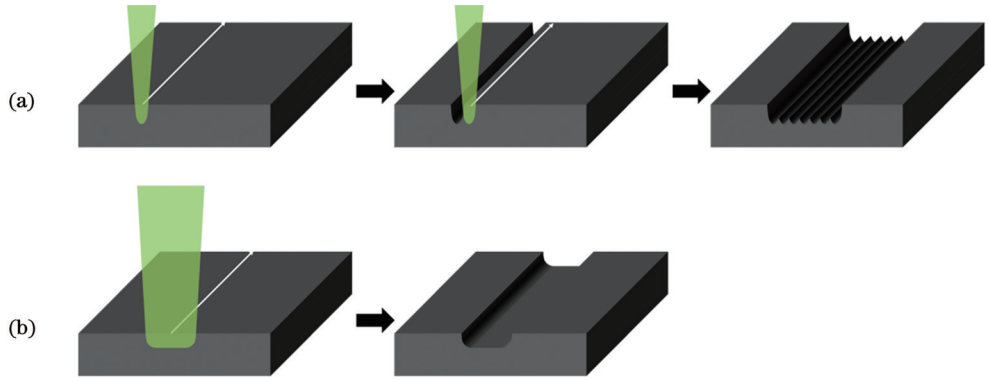

图 5　高斯光斑多次扫描与平顶光斑单次扫描工艺对比。(a)高斯光斑多次扫描工艺；(b)平顶光斑单次扫描工艺

Fig. 5　Comparison of multiple scanning process of Gaussian spot and single scanning process of flat top spot. (a) Multiple scanning process of Gaussian spot; (b) single scanning process of flat top spot

在二维模型中引入平顶高斯分布函数以模拟方平顶光斑的能量分布，即式(12)中 $f_1(x,y)$ 可以表示为

$$f_1(x,y)\big|(y=0)=\exp\left[-\frac{(n+1)x^2}{r_0^2}\right]\sum_{k=1}^{n}\frac{1}{k!}\left[\frac{(n+1)x^2}{r_0^2}\right]^k,\ n=0,1,2,\ldots, \tag{14}$$

式中：r_0 为束腰宽度；n 为高斯函数阶数；k 为函数的迭代变量。当 $n=0$ 时，函数退化为高斯函数。当 $r_0=21\ \mu m$，$n=0,4,16$ 时，分布函数如图 6 所示。

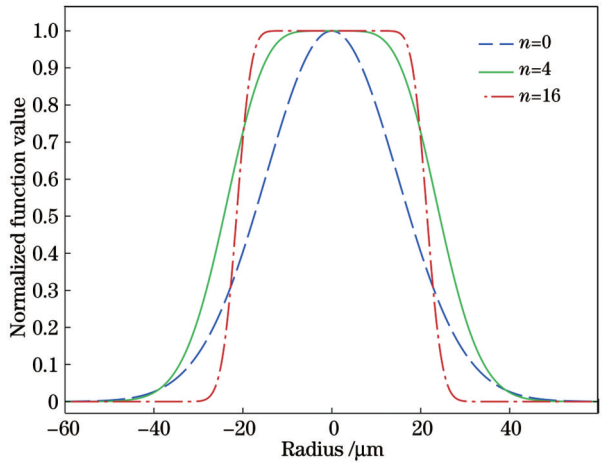

图 6　不同阶平顶高斯分布函数的对比

Fig. 6　Comparison of flat-top Gaussian distribution functions with different orders

n 的取值越大，函数图象越接近标准的平顶分布。取图 6 中 $n=16$ 的平顶高斯分布函数作为平顶光斑分布函数，基于硅的熔点，模拟一个边长为 42 μm、脉冲宽度为 250 fs、脉冲频率为 2 MHz、光通量为 0.5 J·cm^{-2} 的平顶方光斑脉冲串对一个尺寸为 200 μm×10 μm 的二维硅模型弹坑的烧蚀情况，如图 7 所示。

由仿真结果可以看到，单脉冲烧蚀深度约为 0.03 μm，槽底形貌平坦，宽度略小于槽顶。当脉冲数增加时，弹坑深度相应增加，当第 10 个脉冲到达后弹坑深度约为 0.29 μm。由于平顶光斑烧蚀均匀，且槽顶开口较宽，后续脉冲烧蚀时能量损失小。当脉冲数较小时，弹坑深度与脉冲数呈线性增加的关系。进一步改变光通量，研究烧蚀弹坑深度与光通量之间的关系，结果如图 8 所示。

由仿真结果可以看到：当激光通量高于 0.3 J·cm^{-2} 时，由于超过损伤阈值，烧蚀深度急剧增加；当高于 1.5 J·cm^{-2} 时，烧蚀深度的增加速率减小，推测主要是受到晶格热容增加的影响。由仿真结果可以验证，当光通量小于 1.5 J·cm^{-2} 时，飞秒激光的烧蚀热效应较小，且烧蚀深度较为稳定。基于以上双温二维模型的多脉冲激光烧蚀模拟结果，可以建立激光开槽过程中槽形演变与激光工艺参数之间的关联，即通过控制主要的激光开槽工艺参数，如激光峰值功率、激光频率、光斑重叠率等，实现对槽形和槽深的调控，以此指导多脉冲飞秒激光开槽硅晶圆工艺的参数优化。

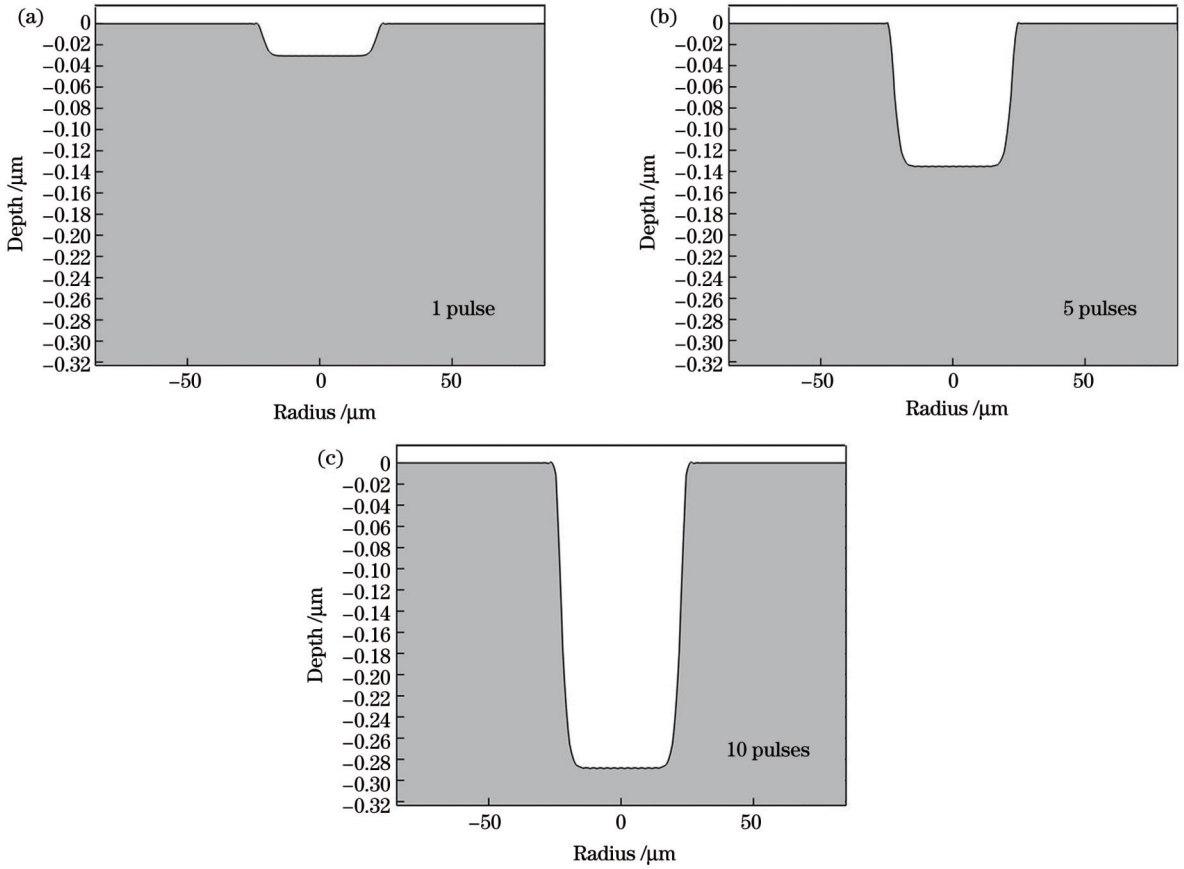

图 7　不同激光脉冲数下的烧蚀弹坑形状。(a)1个脉冲;(b)5个脉冲;(c)10个脉冲

Fig. 7　Ablative crater shapes under different laser pulse numbers. (a) 1 pulse; (b) 5 pulses; (c) 10 pulses

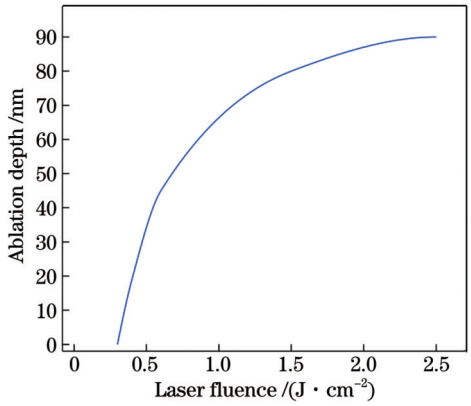

图 8　烧蚀弹坑深度与光通量之间的关系

Fig. 8　Ablation crater depth versus laser fluence

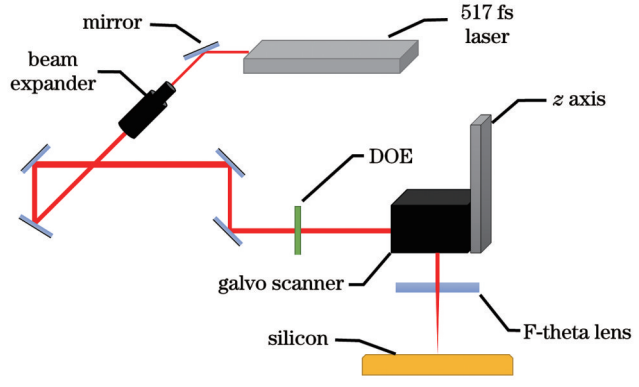

图 9　平顶开槽实验光路图

Fig. 9　Optical path diagram of flat-top laser grooving experiment

3　光路搭建与实验

图 9 给出了飞秒平顶激光开槽光路图。实验中选用中心波长为 517 nm 的飞秒激光器作为光源。利用反射镜组和扩束镜以满足 DOE 元件对激光入射的要求，光束经过 DOE 整形后进入振镜加工系统，并被 F-theta 场镜聚焦于材料表面，通过调整 z 轴位置可以调整焦点相对表面的位置。

为保证激光器 2 MHz 频率的稳定输出，脉宽设定为 250 fs。振镜经过场镜输出校准后可以设定加工速度。在实际加工中通过改变加工速度和输出功率来改变加工工艺参数。由于激光扫描速度与激光频率恒定，单次扫描中单位长度上的脉冲数恒定，采用束腰宽度为 42 μm 的平顶方形光斑，在 2000 mm/s 扫描速度下光斑间隔为 1 μm，脉冲叠加率为 42 pulse/spot，如图 10 所示。加工过程中测得加工位置附近的激光功率为 22.3 W，则平顶光斑焦点位置处的光通量约为 0.62 J·cm^{-2}。根据 2D 模型预测单光斑烧蚀深度约为 0.042 μm，设计开槽深度约为 17 μm，则加工次数设定为 10。最终平顶光斑在晶圆切割道表面开槽的结果如图 11 所示，切割道表面为纯硅。

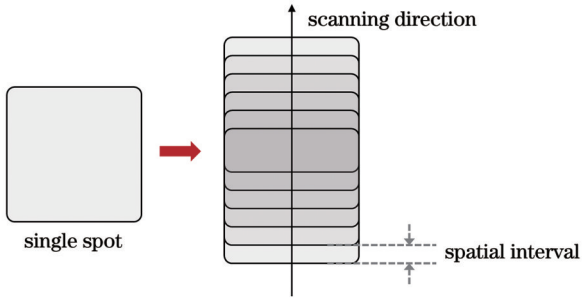

图 10 平顶光斑扫描加工过程中的光斑重叠率及光斑间隔

Fig. 10 Spot overlap rate and spot interval during flat top spot scanning

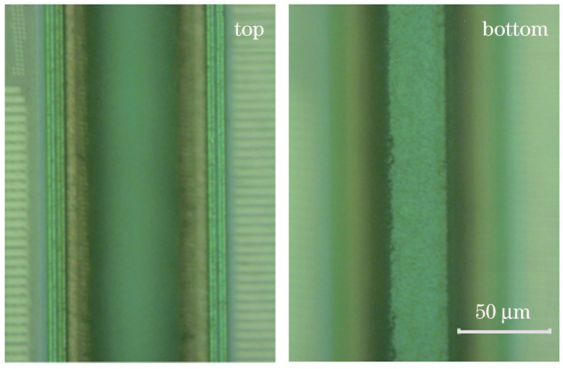

图 11 同一位置处的槽表面和槽底图像

Fig. 11 Groove surface and bottom images at same location

通过光学观察可以发现，平顶光斑开槽后表面边缘锋利，熔融物较少，槽底平整光滑、水平度高。同一位置由激光共聚焦显微镜所测得的开槽表面形貌如图 12 所示。

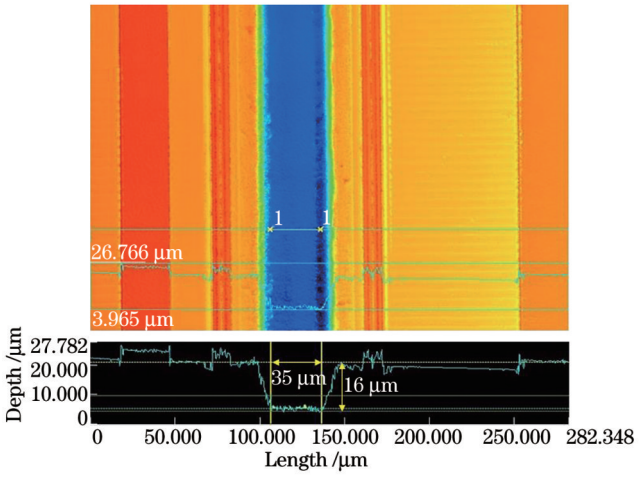

图 12 2D 槽形测试结果

Fig. 12 2D groove shape test result

由激光共聚焦观察结果可以看到，由于采用的激光频率高，光斑间隔小，平顶方光斑烧蚀后槽底平坦，宽度约为 35 μm，侧壁垂直，整体呈倒梯形，槽深约为 16 μm，槽形一致性好。根据 2D 模型预测，单点烧蚀次数为 420，总槽深约为 17.64 μm。烧蚀深度的数值结果略大于实际的加工深度，这是由于实际加工过程中光斑无法达到理想的平顶分布，并且加工过程中材料表面产生的等离子体团会对后续脉冲传输造成影响。当加工脉冲数较少时，本文模型预测的弹坑形状是有效和精确的。

4 结 论

利用 DOE 元件将波长为 517 nm 的飞秒高斯光斑整形为平顶方光斑，实现了硅表面的激光开槽。首先建立了飞秒激光烧蚀硅材料的理论模型。仿真结果表明，飞秒激光可在脉宽时间尺度内激发出大量的自由电子，电子系统温度超过损伤阈值，此时晶格的温度几乎不变。利用平顶高斯分布函数建立了二维平顶光斑的烧蚀模型，计算了激光单脉冲烧蚀深度。结果表明，平顶方光斑烧蚀槽形接近倒梯形，光斑能量利用率高，在脉冲数较小时烧蚀深度与脉冲数呈线性关系。利用自行搭建的硅晶圆飞秒开槽系统，在恒定激光频率下，通过改变振镜加工速度和激光功率来调整开槽工艺。在入射光功率为 22 W、位移台速度为 2000 mm/s 的条件下，获得了槽底水平度高、侧壁垂直度好且深度为 16 μm 的硅晶圆烧蚀槽。实验证明，采用平顶激光开槽可以极大地提高加工效率和光斑利用率，且槽形底部平整，侧壁垂直，有利于后续加工工艺。

参 考 文 献

[1] Atabaki A H, Moazeni S, Pavanello F, et al. Integrating photonics with silicon nanoelectronics for the next generation of systems on a chip[J]. Nature, 2018, 556(7701): 349-354.

[2] Jiang Y W, Li X J, Liu B, et al. Rational design of silicon structures for optically controlled multiscale biointerfaces[J]. Nature Biomedical Engineering, 2018, 2(7): 508-521.

[3] Wang J K, Daineka D, Elyaakoubi M, et al. Microcrystalline silicon thin film deposition from silicon tetrafluoride: isolating role of ion energy using tailored voltage waveform plasmas[J]. Solar Energy Materials and Solar Cells, 2019, 190: 65-74.

[4] Yin Y K, Gao Y F, Li X Y, et al. Experimental study on slicing photovoltaic polycrystalline silicon with diamond wire saw[J]. Materials Science in Semiconductor Processing, 2020, 106: 104779.

[5] Li H S, Gao Y F, Ge P Q, et al. Study on process parameters of fabrication fine diameter electroplated diamond wire for slicing crystalline silicon solar cell[J]. The International Journal of Advanced Manufacturing Technology, 2020, 106(7): 3153-3175.

[6] Samant A N, Dahotre N B. Laser machining of structural ceramics: a review[J]. Journal of the European Ceramic Society, 2009, 29(6): 969-993.

[7] Rihakova L, Chmelickova H. Laser micromachining of glass, silicon, and ceramics[J]. Advances in Materials Science and Engineering, 2015, 2015: 1-6.

[8] Bao J D, Long Y H, Tong Y Q, et al. Experiment and simulation study of laser dicing silicon with water-jet[J]. Applied Surface Science, 2016, 387: 491-496.

[9] Podpod A, Inoue F, De Wolf I, et al. Investigation of advanced dicing technologies for ultra low-k and 3D integration[C]//2016 IEEE 66th Electronic Components and Technology Conference (ECTC), May 31-June 3, 2016, Las Vegas, NV, USA. New York: IEEE Press, 2016: 1247-1258.

[10] Kumagai M, Uchiyama N, Ohmura E, et al. Advanced dicing technology for semiconductor wafer: stealth dicing[J]. IEEE

Transactions on Semiconductor Manufacturing, 2007, 20(3): 259-265.
[11] Suzuki N, Ohba T, Kondo Y, et al. High throughput and improved edge straightness for memory applications using stealth dicing[C] //2018 IEEE 68th Electronic Components and Technology Conference (ECTC), May 29-June 1, 2018, San Diego, CA, USA. New York: IEEE Press, 2018: 2180-2185.
[12] Ohmura E, Kumagai M, Nakano M, et al. Analysis of processing mechanism in stealth dicing of ultra thin silicon wafer[J]. Proceedings of International Conference on Leading Edge Manufacturing in 21st Century: LEM21, 2007, 4: 9D435.
[13] Kumagai M, Sakamoto T, Ohmura E. Laser processing of doped silicon wafer by the Stealth Dicing[C] //2007 International Symposium on Semiconductor Manufacturing, October 15-17, 2007, Santa Clara, CA, USA. New York: IEEE Press, 2008.
[14] 张怀智, 徐家明, 张兰天, 等. 硅晶圆多焦点激光隐切算法与实验[J]. 中国激光, 2022, 49(2): 0202018.
Zhang H Z, Xu J M, Zhang L T, et al. Algorithm and experiment of silicon wafer multifocus laser stealth dicing[J]. Chinese Journal of Lasers, 2022, 49(2): 0202018.
[15] Galasso G, Kaltenbacher M, Tomaselli A, et al. A unified model to determine the energy partitioning between target and plasma in nanosecond laser ablation of silicon[J]. Journal of Applied Physics, 2015, 117(12): 123101.
[16] Noh J, Kim J H, Sohn H, et al. Comparison of bending fracture strength of silicon after ablation with nanosecond and picosecond lasers[J]. The International Journal of Advanced Manufacturing Technology, 2016, 84(9): 2029-2036.
[17] Ali J M Y, Shanmugam V, Khanna A, et al. Analysis of nanosecond and femtosecond laser ablation of rear dielectrics of silicon wafer solar cells[J]. Solar Energy Materials and Solar Cells, 2019, 192: 117-122.
[18] de Menezes R F, Harvey C M, de Martínez Gerbi M E M, et al. Fs-laser ablation of teeth is temperature limited and provides information about the ablated components[J]. Journal of Biophotonics, 2017, 10(10): 1292-1304.
[19] Ngoi B K A, Venkatakrishnan K, Lim E N L, et al. Effect of energy above laser-induced damage thresholds in the micromachining of silicon by femtosecond pulse laser[J]. Optics and Lasers in Engineering, 2001, 35(6): 361-369.
[20] Fornaroli C, Holtkamp J, Gillner A. Dicing of thin silicon wafers with ultra-short pulsed lasers in the range from 200 fs up to 10 ps [J]. Journal of Laser Micro, 2015, 10(2): 229-233.
[21] Mottay E, Liu X B, Zhang H B, et al. Industrial applications of ultrafast laser processing[J]. MRS Bulletin, 2016, 41(12): 984-992.
[22] Crawford T H R, Borowiec A, Haugen H K. Femtosecond laser micromachining of grooves in silicon with 800 nm pulses[J]. Applied Physics A, 2005, 80(8): 1717-1724.
[23] Domke M, Egle B, Piredda G, et al. Ultrashort pulse laser dicing of thin Si wafers: the influence of laser-induced periodic surface structures on the backside breaking strength[J]. Journal of Micromechanics and Microengineering, 2016, 26(11): 115004.
[24] Amer M S, El-Ashry M A, Dosser L R, et al. Femtosecond versus nanosecond laser machining: comparison of induced stresses and structural changes in silicon wafers[J]. Applied Surface Science, 2005, 242(1/2): 162-167.
[25] Shi K W, Yow K Y, Lo C. Single & multi beam laser grooving process parameter development and Die strength characterization for 40 nm node low-K/ULK wafer[C] //2014 IEEE 16th Electronics Packaging Technology Conference (EPTC), December 3-5, 2014, Singapore. New York: IEEE Press, 2015: 752-759.
[26] Glezer E N, Huang L, Siegal Y, et al. Phase transitions induced by femtosecond pulses[J]. MRS Online Proceedings Library, 1995, 397(1): 3-20.
[27] Domke M, Egle B, Stroj S, et al. Ultrafast-laser dicing of thin silicon wafers: strategies to improve front- and backside breaking strength[J]. Applied Physics A, 2017, 123(12): 746.
[28] Taylor L L, Scott R E, Qiao J. Integrating two-temperature and classical heat accumulation models to predict femtosecond laser processing of silicon[J]. Optical Materials Express, 2018, 8(3): 648-658.

Simulation and Experimental Research on Flat Top Femtosecond Laser Grooving of Silicon Wafer

Zhang Zhe[1,2], Song Qi[1,3], Zhang Kunpeng[1], Xue Mei[1], Hou Yu[1**], Zhang Zichen[1*]

[1]*Microelectronics Instruments and Equipment R&D Center, Institute of Microelectronics, Chinese Academy of Sciences, Beijing* 100029, *China*;

[2]*School of Microelectronics, University of Chinese Academy of Sciences, Beijing* 100049, *China*;

[3]*International Research Centre for Nano Handling and Manufacturing of China, Changchun University of Science and Technology, Changchun* 130022, *Jiling, China*

Abstract

Objective Silicon is an important material utilized in various fields, such as biology and energy, particularly in the realm of integrated circuits. With advancements in semiconductor manufacturing toward large formats and thin substrates, the wafer-edge chipping and damage caused by traditional blade dicing have become increasingly significant in the field of semiconductor packaging. The introduction of low-dielectric-constant materials in the 90 nm integrated circuit technology node has presented a significant challenge to wafer dicing processes. The industry has responded by implementing a combination of laser surface grooving and mechanical dicing to address the low-dielectric-constant material separation issue. Laser processing equipment manufacturers have redirected their focus from nanosecond laser processing equipment toward ultrafast laser processing equipment that offers reduced thermal affected zones. However, existing research mainly focuses on optimizing the laser power, frequency, defocus, and feed speed, and comparatively analyzes multi-beam laser scribing spot distributions. A comprehensive theoretical analysis remains lacking. To address this gap, the current study utilizes a 517 nm femtosecond laser as a light source and shapes the energy of the focal spot into a flat-top distribution via a diffractive optical element for the surface grooving of silicon materials. The mechanism and quality of the

groove process are investigated and discussed.

Methods The experimental setup comprises a diode-pumped femtosecond fiber laser as the light source, while a galvanometer and an F-theta lens served as the beam movement and focusing tools. A diffractive optical element (DOE) is used to shape the near-focus spot into a top-hat square distribution on the surface of silicon for grooving. First, a one-dimensional simulation model is established using finite element analysis software, and the dual-temperature model is coupled with the excess carrier balance equation to analyze the interdependence among the material electrons, lattice, and carrier density in the femtosecond laser ablation process. This results in the establishment of a theoretical model for the femtosecond laser ablation process for silicon materials. Subsequently, a two-dimensional simulation model is established to simulate the morphology evolution during the silicon laser ablation process, and the impact of multipulse lasers with different spot intervals and energies on the groove quality is calculated. Finally, an experimental optical system is constructed for the grooving experiments, and the actual morphology is tested using a laser confocal microscope and the results are compared with those of the two-dimensional simulation.

Results and Discussions The one-dimensional model (Fig. 1) demonstrates that the temperature of the free electrons in the silicon material increases rapidly during the 517 nm femtosecond laser irradiation, reaching a maximum temperature of approximately 28000 K, while the lattice temperature remains constant. The energy of the electrons is transferred to the lattice system after the laser pulse, causing the temperature of the electrons to decrease and that of the lattice to increase (Fig. 2). This suggests that the femtosecond laser primarily damages the silicon material through electron excitation, thereby achieving "cold" processing and reducing thermal damage to the material. The two-dimensional model (Fig. 7) demonstrates that ablation occurs when the laser flux exceeds 0.3 $J\cdot cm^{-2}$ and the ablation depth increases significantly. The simulation results indicate that the thermal effect of the femtosecond laser ablation is small when the luminous flux is below 1.5 $J\cdot cm^{-2}$, and the ablation depth remains relatively stable (Fig. 8). The experimental results confirm that the top-hat square spot produces a flat-bottomed inverted trapezoidal groove with a width of approximately 35 μm and a depth of approximately 16 μm (Fig. 11). The sidewalls of the grooves are vertical and their shapes are consistent. However, the actual groove depth is slightly smaller than the depth calculated from the two-dimensional simulation model owing to the non-ideal fluence distribution of the light spot and the presence of plasma clusters generated during processing. These results indicate that the model produces better results with fewer processing pulses.

Conclusions This study proposes the use of a DOE element to shape a femtosecond Gaussian spot with a wavelength of 517 nm into a top-hat square spot to achieve laser grooving on silicon surfaces. First, a theoretical model for the femtosecond laser ablation of silicon materials is established. The simulation results demonstrate that the femtosecond laser can excite a significant number of free electrons within the pulse duration, causing the electronic system temperature to surpass the damage threshold, while the crystal lattice temperature remains constant. A flat-top Gaussian distribution function is utilized to establish a two-dimensional flat-top spot ablation model, and the laser single-pulse ablation depth is calculated. The results indicate that the ablation groove shape of the flat-top square spot closely resembles an inverted trapezoid, with a high energy utilization rate and a linear relationship between the ablation depth and the number of pulses when the number of pulses is small. A self-constructed silicon wafer femtosecond grooving system is used to adjust the grooving process by modifying the processing speed of the galvanometer and laser power at a constant laser frequency. Under the conditions of an incident light power of 22 W and a stage speed of 2000 mm/s, silicon wafer grooving is obtained with a high groove bottom level, good side wall verticality, and a depth of 16 μm. The experiments demonstrate that the use of flat-top laser grooving significantly improves the processing efficiency and spot utilization, with a flat groove bottom and vertical side wall, which are advantageous for subsequent processing technologies.

Key words laser technique; femtosecond laser; two temperature model; beam shaping; laser ablation; wafer dicing